

SunQM-3s3: Using QM calculation to explain the atmosphere band pattern on Jupiter (and Earth, Saturn, Sun)'s surface

Yi Cao

Ph.D. of biophysics, a citizen scientist of QM.

E-mail: yicaojob@yahoo.com

© All rights reserved

The major part of this work was done in Dec. 2016.

Abstract

Using $p\{N,n\}$ QM model with QM induced mass peaking/depleting effect, plus the spin frame of $\omega_{n\text{-spin}} \approx \omega_{1\text{-spin}} / n^3$, plus the multiplier n' , I successfully explained the origin of Jupiter surface cloud bands as the $|544\rangle$ zonal bands embedded in the background $|400\rangle$ belt bands. We can even calculate out how deep the convection starts below the atmosphere surface. The Earth's atmospheric circulation is also caused by the same QM peaking/depleting effect of $|211\rangle$ state on top (not embedded) of $|100\rangle$ state, which generates a major upwelling band at equator and two minor upwelling bands at $\pm 60^\circ$ latitude, and two down welling bands at $\approx \pm 35^\circ$ latitude. The same QM theory is applicable to all other planets' atmosphere, even for the Sun's surface atmosphere.

Introduction

The famous and characteristic cloud bands of Jupiter's atmosphere makes physicists wonder how it has been formed. This paper presents how I tried to solve this problem by using Schrodinger equation and my newly discovered $\{N,n\}$ QM theory. The result looks quite promising. Then I will try to extend the same method to Earth's atmosphere circulation and even to Sun's atmosphere. Note: for $\{N,n\}$ QM nomenclature as well as the general notes for $\{N,n\}$ QM model, please see my paper SunQM-1 section VII. Note: Microsoft Excel's number format is often used in this paper, for example: $x^2 = x^2$, $3.4E+12 = 3.4*10^{12}$, $5.6E-9 = 5.6*10^{-9}$.

I. Schrodinger equation and solution for Jupiter: surface atmosphere bands and the body construction

I-a. Using QM calculation to explain the cloud bands in Jupiter's atmosphere

From paper SunQM-1^[1], we know that Solar system can be described by a $\{N,n//6\}$ QM structure, where Sun surface ends at $\{0,2\}$, Earth's orbit at $\{1,5\}o$, and Jupiter's orbit at $\{2,2\}o$. Inside the Sun ball, its QM structure can be described by the interior $\{N,n//6\}$ QM structure. Similarly, from paper SunQM-1s3, we know that Jupiter can be described by a $p\{N,n//5\}$ QM structure, which means not only its moon's orbits can be described by the exterior $p\{N,n//5\}$ QM, its internal structure (mainly the inner core) can also be described by the interior $p\{N,n//5\}$ QM. Let us set $p\{0,1//5\}$ at Jupiter's surface. Jupiter atmosphere's cloud bands locate just on the surface. So it is also at $p\{0,1//5\}$.

From paper SunQM-3, we know that Sun's $\{N,n\}$ QM structure can be described by the Schrodinger equation. Similarly, Jupiter's $\{N,n\}$ QM structure can also be described by Schrodinger equation. So now let us build a model for Jupiter's Schrodinger equation: Let us define r_1 at Jupiter's Earth-sized core $p\{-1,1//5\}$. The mass outside the core is composed by n shells ($n = 1, 2, 3, 4$), with the most outer $n = 4$ orbit shell ends at $n = 5$ (or $p\{-1,5\}$, or $r/r_1 = 25$). Each n shell is composed by a number of l sub-shells, $l = 0, 1, \dots, n-1$, with $l = 0$ sub-shell at the most outside (see from Figure 1a). Besides that, at the surface of $r/r_1 = 25$, there is also a significant amount of contribution from $|5,4,m\rangle$ state, and small

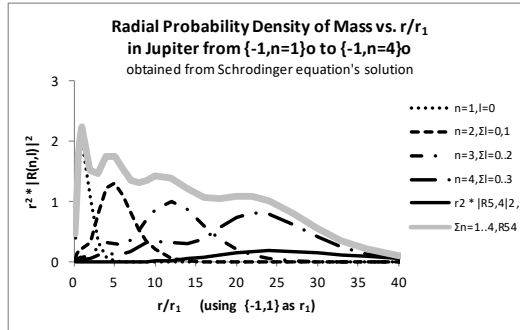
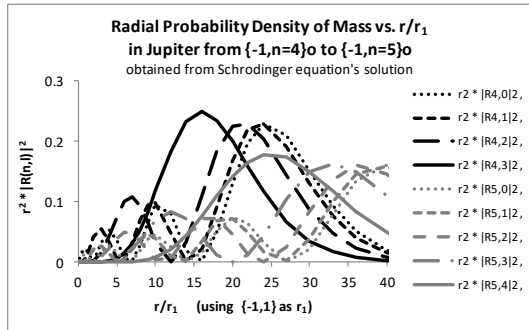
contribution from $|5,3,m\rangle$, $|5,2,m\rangle$, $|5,1,m\rangle$, $|5,0,m\rangle$ states (see from Figure 1a). In our simplified model, I only include $|5,4,m\rangle$ state, and ignored the rest $n = 5$ states. So count the QM states of each sub-shell in Jupiter's $p\{-1,n=1..5\}$ o super-shell from surface to center, they are: $|5,4,m\rangle$, $|4,0,m\rangle$, $|4,1,m\rangle$, $|4,2,m\rangle$, $|4,3,m\rangle$, $|3,0,m\rangle$, $|3,1,m\rangle$, $|3,2,m\rangle$, $|2,0,m\rangle$, $|2,1,m\rangle$, $|1,0,m\rangle$. The out-most sub-shell (at state $|54m\rangle$, where the Jupiter's atmosphere located) has Schrodinger equation solution $|R(5,4)|^2 * |Y(4,m=-4...+4)|^2$.

Now let us first plot the radial mass density probability distribution $r^2 * |R(5,l=0...4)|^2$ along r/r_1 . Figure 1a shows the Jupiter's radial probability density vs. r/r_1 from $n = 4$ shell (or $p\{-1,4\}$ o) to $n = 5$ shell (or $p\{-1,5\}$ o). Figure 1b shows the Jupiter's radial probability density for $n = 1, 2, 3, 4$ shells and $|54m\rangle$ sub-shell. Figure 1c shows the $r/r_1 \geq 25$ compressed $r^2|R(n,l)|^2$ vs. r/r_1 plot for Jupiter's $\{-1,1\}$ to $\{-1,5\}$ structure (calculated as $r/r_1 = 25 + \log(r/r_1 - 25)$).

Table 1. $r^2 * |R(n,l)|^2$ vs. r/r_1 for $n = 1$ to 5 .

$a_0 =$	0.280 E+7 meters													r cut-off=		
$r/a_0 =$	$r^2 * R_{4,0} ^2$	$r^2 * R_{4,1} ^2$	$r^2 * R_{4,2} ^2$	$r^2 * R_{4,3} ^2$	$r^2 * R_{4,4} ^2$	$r^2 * R_{5,0} ^2$	$r^2 * R_{5,1} ^2$	$r^2 * R_{5,2} ^2$	$r^2 * R_{5,3} ^2$	$r^2 * R_{5,4} ^2$	$n=2, \Sigma l=0$	$n=3, \Sigma l=0$	$n=4, \Sigma l=0$	$n=5, \Sigma l=0$	$\Sigma n=1..4, R$	$\log(r/a_0) =$
0.2	0.005905	3.04E-05	9.76E-09	4.007E-13	0.003023	1.59E-05	5.73E-09	3.442E-13	3.9E-18	0.38304	0.047564	0.014076	0.005936	0.003038	0.450616	0.2
0.4	0.015144	0.000397	5.46E-07	9.283E-11	0.007743	0.00208	3.21E-07	7.971E-11	3.69E-15	1.027038	0.125126	0.036899	0.015541	0.007951	1.204605	0.4
0.6	0.020996	0.00163	5.44E-06	2.153E-09	0.010712	0.000853	3.19E-06	1.847E-09	1.96E-13	1.548999	0.18346	0.053828	0.022631	0.011569	1.808917	0.6
0.8	0.021819	0.004168	2.67E-05	1.946E-08	0.011094	0.002178	1.56E-05	1.669E-08	3.22E-12	1.845911	0.212254	0.061975	0.026013	0.013288	2.146153	0.8
1	0.018514	0.008199	8.89E-05	1.049E-07	0.00936	0.004277	5.2E-05	8.99E-08	2.77E-11	1.933361	0.218976	0.063869	0.026802	0.013689	2.243008	1
2	0.00057	0.0414	0.002851	1.629E-05	0.000361	0.021192	0.00165	1.385E-05	1.9E-08	1.046608	0.322227	0.103617	0.044838	0.023217	1.517289	2
3	0.031627	0.055222	0.015956	0.0002533	0.016491	0.027053	0.009046	0.0002122	7.34E-07	0.318697	0.800149	0.24346	0.103058	0.052803	1.465365	3
4	0.053704	0.032223	0.042964	0.0015344	0.026527	0.014151	0.023574	0.0012584	8.74E-06	0.076677	1.221043	0.32227	0.130425	0.065519	1.750424	4
5	0.034904	0.00466	0.076108	0.0055472	0.015467	0.001146	0.039772	0.0044191	5.46E-05	0.016214	1.303472	0.303581	0.121219	0.060858	1.744541	5
6	0.006251	0.003751	0.101269	0.014467	0.001702	0.003757	0.049264	0.0110953	0.000226	0.00316	1.115438	0.286848	0.125738	0.066044	1.531411	6
7	0.002589	0.031873	0.107559	0.0301165	0.00298	0.020352	0.047016	0.0220104	0.000709	0.000582	0.824493	0.35429	0.172138	0.093068	1.352212	7
8	0.029072	0.069774	0.093032	0.053161	0.019006	0.038239	0.034336	0.0365865	0.001807	0.000103	0.54952	0.509386	0.245039	0.129973	1.305855	8
9	0.067131	0.095592	0.064346	0.0827306	0.037235	0.045821	0.017528	0.0528745	0.003933	1.76E-05	0.339157	0.701133	0.3098	0.157392	1.35404	9
10	0.094261	0.097917	0.032639	0.1165679	0.045586	0.039694	0.004253	0.0680461	0.007561	2.94E-06	0.197274	0.869076	0.341385	0.165139	1.415298	10
12	0.079674	0.047805	0	0.1843888	0.025239	0.008952	0.006656	0.0841391	0.021035	7.77E-08	0.058458	0.997939	0.311867	0.14602	1.389299	12
14	0.020017	0.002036	0.03326	0.2328168	0.000614	0.002845	0.041056	0.0729893	0.044154	1.94E-09	0.015231	0.859702	0.288129	0.161659	1.207217	14
16	0.00213	0.020447	0.109052	0.2492617	0.014687	0.033756	0.071347	0.0424206	0.075414	4.63E-11	0.003618	0.608122	0.380891	0.237625	1.068046	16
18	0.050344	0.09112	0.182994	0.2352779	0.052124	0.067398	0.071406	0.0122265	0.110038	1.07E-12	0.000802	0.373498	0.559736	0.313192	1.044074	18
20	0.130164	0.168899	0.225198	0.2010697	0.074224	0.072701	0.044867	0	0.141802	2.43E-14	0.000168	0.206363	0.725331	0.333594	1.073665	20
22	0.197357	0.218557	0.229322	0.15856	0.0637	0.048905	0.014026	0.0122922	0.165262	5.38E-16	3.38E-05	0.105026	0.803797	0.304185	1.074119	22
24	0.228301	0.229407	0.20476	0.1170059	0.032916	0.017285	4.33E-05	0.0443164	0.177266	1.17E-17	6.56E-06	0.050055	0.779475	0.271826	1.006802	24
27	0.209445	0.191538	0.144724	0.0669863	0.000492	0.001364	0.025395	0.1048835	0.173379	3.68E-20	5.31E-07	0.014936	0.612692	0.305513	0.801008	25.30
30	0.151338	0.129989	0.087499	0.034722	0.02126	0.038829	0.084244	0.1497675	0.149768	1.13E-22	4.08E-08	0.004062	0.403548	0.443868	0.557378	25.70
33	0.092823	0.076191	0.047077	0.0166075	0.078899	0.099697	0.13714	0.1634152	0.117001	3.38E-25	3E-09	0.001027	0.232699	0.596153	0.350728	25.90
36	0.050442	0.039993	0.023125	0.0074331	0.13351	0.146205	0.160659	0.1495549	0.084125	9.96E-28	2.13E-10	0.000245	0.120994	0.674053	0.205363	26.04
40	0.019398	0.014845	0.008016	0.0023369	0.16105	0.159224	0.146525	0.1095997	0.048711	4.13E-31	6E-12	3.35E-05	0.044596	0.62511	0.093341	26.18
45	0.004943	0.00366	0.001853	0.0004922	0.129662	0.118957	0.095408	0.0594649	0.021407	2.37E-35	6.53E-14	2.54E-06	0.010948	0.42449	0.032358	26.30
50	0.00109	0.000787	0.000379	9.385E-05	0.076746	0.067074	0.049064	0.0269212	0.008309	1.33E-39	6.75E-16	1.77E-07	0.002351	0.228114	0.01066	26.40
55	0.000215	0.000152	7.07E-05	1.651E-05	0.036887	0.031137	0.021302	0.0106302	0.002917	7.3E-44	6.7E-18	1.15E-08	0.000455	0.102873	0.003371	26.48
60	3.89E-05	2.71E-05	1.22E-05	2.719E-06	0.015217	0.012511	0.008131	0.0037692	0.000942	3.94E-48	6.42E-20	7.1E-10	8.09E-05	0.04057	0.001023	26.54
65	6.54E-06	4.5E-06	1.97E-06	4.234E-07	0.005579	0.004492	0.002803	0.0012248	0.000284	2.1E-52	5.98E-22	4.18E-11	1.34E-05	0.014383	0.000297	26.60
70	1.04E-06	7.05E-07	3.02E-07	6.288E-08	0.001861	0.001474	0.000889	0.0003702	8.06E-05	1.11E-56	5.44E-24	2.37E-12	2.11E-06	0.004675	8.27E-05	26.65

Note: use Jupiter inner core $p\{-1,1/5\}$ as r_1 ($= a_0$ in formula), which is $1/25$ of Jupiter surface $p\{0,1/5\}$'s r , $r_1 = 6.99E+7 / 25 = 0.280E+7$ m.



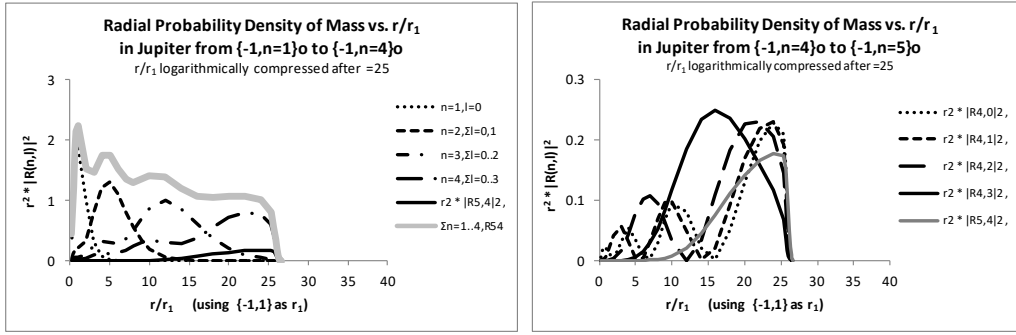


Figure 1a (top-left). The original $r^2 * |R(n,l)|^2$ vs. r/r_1 plot for Jupiter's $\{-1,n=4\}$ to $\{-1,n=5\}$ structure in r -dimension.
 Figure 1b (top-right). The radial probability density $r^2 * |R(n,l)|^2$ vs. r/r_1 plot for Jupiter's $n=1, 2, 3, 4$ shell, and $|54m\rangle$ sub-shell.
 Figure 1c (bottom-left). The $r/r_1 \geq 25$ compressed $r^2 * |R(n,l)|^2$ vs. r/r_1 plot for Figure 1b.
 Figure 1d (bottom-right). Same as Figure 1a, except the r/r_1 is compressed at ≥ 25 . Only $|40m\rangle, |41m\rangle, |42m\rangle, |43m\rangle,$ and $|54m\rangle$ states are displayed.

The original radial wave function $R(n,l)$ extends r/r_1 from 0 to infinity, and we know that for Jupiter a boundary condition need to be added. Since I am only the citizen level QM scientist, I do not know what boundary condition is correct, so I simply make a logarithmically compression at $r/r_1 \geq 25$, so it becomes $25 + \log(r/r_1 - 25)$. Why choose $r/r_1 = 25$ to cut-off? Because Jupiter's surface is at $n = 5$, so $r/r_1 = n^2 = 25$, therefore it needs to cut-off at 25 to make the probability quickly drop to zero.

In paper SunQM-3, we learned the nLL effect: the spinning of Sun removed the degeneracy of n orbital energy levels, so the nLL state has the lowest E level among all $|nlm\rangle$ states in each n shell. The same thing happens to Jupiter too. The spinning of Jupiter removed the degeneracy of orbital energy levels, so that for $n = 5$ shell, the $|nLL\rangle = |544\rangle$ state has the lowest E level among all $l (= 0 \dots 4)$ and all $m(s)$.

Figure 1 shows that $n = 1, 2, 3, 4$ are spherical shells of orbits with increasing r . We can see that all n shells are overlap with each other a lot. Now let us simplify the Jupiter QM model structure by assuming that n -shells are solid bodies, so they can not overlap on each other. From paper SunQM-3s2, we learned that (the simplified rule can be) all mass between r_n and r_{n+1} belong to orbit n . So let us assume that $n = 1$ (solid body) shell covers r/r_1 from 1 to 4, $n = 2$ solid shell covers r/r_1 from 4 to 9, $n = 3$ solid shell covers r/r_1 only from 9 to 16, $n = 4$ solid shell covers r/r_1 only from 16 to 25. A (possible) out-most solid shell of $n = 5$ covers r/r_1 from 25 to 36, but this r/r_1 is log-compressed to $\Delta(r/r_1) = \log(36) - \log(25) \approx 0.158$. It equivalent to $0.158/25 \approx 0.63\%$ of Jupiter's radius, or a thickness of 440 km at Jupiter's surface (see Figure 1d). Remember that in our simplified model, only $|54m\rangle$ states make contribution in $n = 5$ shell. Its mass probability density is determined by Schrodinger equation solutions: $r^2 * |R(5,4)|^2 * |Y(4,m)|^2 * \sin(\theta)$. Since we only interested in the Jupiter's surface, then the whole question is simplified as that we only need to figure out the mass density distribution in $\theta\phi$ -2D-dimension, which is determined by $|Y(4,m)|^2 * \sin(\theta)$. Since $|Y(l,m)|^2 * \sin(\theta)$ is always ϕ -dimension degenerated, so the question is further simplified to be in θ -dimension only.

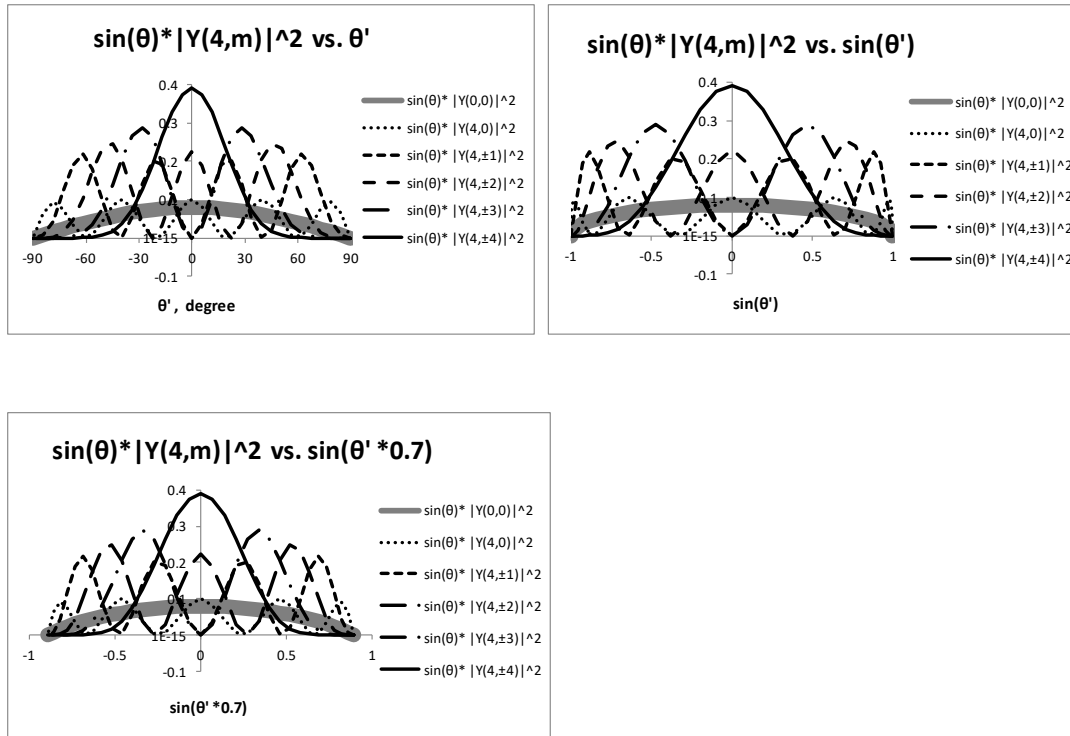
We can also simplify the l sub-shells as solid shells. So underneath the $|54m\rangle$ solid sub-shell is the $|400\rangle$ solid sub-shell. Now I need to show the θ' dependency of $|Y(4,m)|^2$. Since

$$\iiint |\Psi_{nlm}^*| |\Psi_{nlm}| r^2 \sin(\theta) dr d\theta d\phi = \iiint |R_{nl}^*| |R_{nl}| * |Y_{lm}^*| |Y_{lm}| r^2 \sin(\theta) dr d\theta d\phi, \tag{Eq-1}$$

and for the radial probability density distribution, all text book use $r^2 * |R(n,l)|^2$ to plot. After some tests, I figured out that using $\sin(\theta) * |Y(4,m)|^2$ is better than use $|Y(4,m)|^2$ along. Figure 2 (and Table 2) shows the plot of $\sin(\theta) * |Y(4,m)|^2$ vs. θ (for $|54m\rangle$ state at $r/r_1 \approx 25$), as well as $\sin(\theta) * |Y(0,0)|^2$ vs. θ (for $|400\rangle$ state at $r/r_1 \approx 25$).

Table 2. Plot of $|Y(4,m)|^2$ vs. θ , as well as $|Y(0,0)|^2$ vs. θ .

		3D projected to 2D		spin caused $y = \sin(\theta^*0.7)$		spin caused $y = \sin(\theta^*0.9)$																				
θ , in π	θ , in arc degree	$y = \sin(\theta)$	$y = \cos(\theta)$	$y = \sin(\theta^*0.7)$	$y = \cos(\theta^*0.7)$	$y = \sin(\theta^*0.9)$	$y = \cos(\theta^*0.9)$	$ Y(0,0) ^2$	$ Y(1,0) ^2$	$ Y(1,\pm 1) ^2$	$ Y(1,m) ^2$	$ Y(2,0) ^2$	$ Y(2,\pm 1) ^2$	$ Y(2,\pm 2) ^2$	$ Y(2,m) ^2$	$ Y(3,0) ^2$	$ Y(3,\pm 1) ^2$	$ Y(3,\pm 2) ^2$	$ Y(3,\pm 3) ^2$	$ Y(3,m) ^2$	$ Y(4,0) ^2$	$ Y(4,\pm 1) ^2$	$ Y(4,\pm 2) ^2$	$ Y(4,\pm 3) ^2$	$ Y(4,\pm 4) ^2$	$ Y(4,m) ^2$
0	0	0	1	0.891007	0.987688	0	0	0	0	0	0	0	0	0	0	0	0	0	0	0	0	0	0	0	0	0
1/32	0.9817	84	0.995185	0.857729	0.970031	0.0078	0.023175	0.0002248	0.0233999	0.037884	0.0011133	2.7E-06	0.0389998	0.051509	0.0030722	1.872E-05	3.026E-08	0.0545997	0.063671	0.00664568	7.127E-05	2.697E-07	3.271E-10	0.0701996		
1/16	0.19635	79	0.980785	0.820401	0.944806	0.015525	0.044802	0.0017726	0.0465744	0.069014	0.0085258	8.433E-05	0.077624	0.08559	0.0225117	0.0005679	3.745E-06	0.1086736	0.093044	0.0445675	0.0020793	3.242E-05	1.603E-07	0.1397232		
3/32	0.29452	73	0.95694	0.779201	0.91221	0.0231	0.063461	0.0058396	0.0693004	0.088148	0.0267377	0.0006151	0.1155006	0.092259	0.0654389	0.0039428	6.047E-05	0.1617008	0.077294	0.1166004	0.0135027	0.0004984	5.732E-06	0.2079011		
1/8	0.3927	68	0.92388	0.734323	0.872496	0.030453	0.07798	0.0133792	0.0913589	0.092716	0.0570993	0.024492	0.1522649	0.07311	0.1250088	0.0146335	0.0004185	0.2131709	0.035836	0.1894957	0.0454616	0.0032145	6.894E-05	0.2740768		
0.49087	62	0.881921	0.685977	0.825975	0.037513	0.08753	0.0250075	0.1125377	0.083364	0.0972525	0.0069463	0.1875628	0.040346	0.1826215	0.0378192	0.0018008	0.2625879	0.003719	0.2179268	0.1029107	0.012606	0.0004502	0.337613			
3/16	0.58905	56	0.83147	0.634393	0.77301	0.044211	0.091694	0.0409382	0.1326326	0.063748	0.1415113	0.0157949	0.2210544	0.011157	0.216194	0.0764376	0.0056878	0.3094761	0.006366	0.179544	0.1746234	0.0353896	0.001975	0.3978979		
7/32	0.68722	51	0.77301	0.579815	0.714015	0.050483	0.090498	0.0609519	0.1514502	0.039647	0.1821075	0.030663	0.2524171	7.95E-06	0.2107211	0.1282576	0.0143972	0.3533839	0.041894	0.0955418	0.2329693	0.0774268	0.0065185	0.4543507		
1/4	0.7854	45	0.707107	0.522499	0.649448	0.05627	0.084405	0.0844047	0.1688093	0.017584	0.2110116	0.0527529	0.2813488	0.012309	0.1661717	0.1846352	0.0307725	0.3938884	0.08358	0.0197823	0.2472793	0.1384764	0.0173095	0.5064279		
9/32	0.88357	39	0.634393	0.462716	0.579815	0.061514	0.07427	0.1102726	0.1845427	0.003306	0.2218986	0.028366	0.3075711	0.042267	0.0988717	0.2320403	0.0574203	0.4305995	0.100276	0.0027811	0.2039892	0.2079818	0.0386002	0.553628		
5/16	0.98175	34	0.55557	0.400749	0.505657	0.066166	0.061268	0.1372305	0.1984987	0.000453	0.2117866	0.0185914	0.3308312	0.07584	0.0354425	0.2562296	0.0956517	0.4631637	0.007074	0.0595976	0.119808	0.2657133	0.074394	0.5954962		
11/32	1.07992	28	0.471397	0.33669	0.427555	0.070181	0.046786	0.1637574	0.2105432	0.009749	0.1819466	0.15921	0.3509053	0.097378	0.0017678	0.2476519	0.1444697	0.4912675	0.037074	0.1423665	0.0368474	0.2889299	0.1264122	0.6316296		
3/8	1.1781	23	0.382683	0.27144	0.346117	0.07352	0.0323	0.1882597	0.22056	0.028888	0.13785	0.2008622	0.3676	0.096899	0.0118108	0.2059091	0.200021	0.51464	0.004271	0.2016121	9.511E-05	0.2636316	0.1920697	0.66168		
13/32	1.27627	17	0.292085	0.20471	0.261979	0.076151	0.019251	0.2092021	0.2284527	0.053145	0.0881423	0.239467	0.3807545	0.074671	0.0612974	0.1412511	0.2558363	0.5330562	0.00556	0.192	0.030212	0.1940229	0.263563	0.685358		
7/16	1.37445	11	0.19509	0.137012	0.175796	0.078048	0.008912	0.2252336	0.2341452	0.076553	0.0428622	0.2708265	0.3902421	0.0411039	0.1292077	0.072154	0.3039385	0.5463889	0.037074	0.1423665	0.0368474	0.2889299	0.1264122	0.6316296		
15/32	1.4762	6	0.098017	0.068668	0.088242	0.079194	0.002283	0.2353003	0.2375829	0.039369	0.0113031	0.2912996	0.3959714	0.011603	0.1865825	0.1959903	0.3365845	0.55436	0.082092	0.0364567	0.1900773	0.0291032	0.3750197	0.7127486		
1/2	1.5708	0	0.13E-17	0	0	0.079577	8.96E-34	0.2387324	0.2387324	0.099472	4.479E-33	0.2984155	0.3978874	4.7E-33	0.2088809	7.839E-33	0.3481514	0.5570423	0.100715	1.512E-32	0.2281116	1.176E-32	0.3916704	0.7161972		
17/32	1.66897	-6	-0.09802	-0.06867	-0.08824	0.079194	0.002283	0.2353003	0.2375829	0.039369	0.0113031	0.2912996	0.3959714	0.011603	0.1865825	0.1959903	0.3365845	0.55436	0.082092	0.0364567	0.1900773	0.0291032	0.3750197	0.7127486		
9/16	1.76715	-11	-0.19509	-0.13701	-0.1758	0.078048	0.008912	0.2252336	0.2341452	0.076553	0.0428622	0.2708265	0.3902421	0.041039	0.1292077	0.072154	0.3039385	0.5463889	0.037074	0.1423665	0.0368474	0.2889299	0.1264122	0.6316296		
19/32	1.86532	-17	-0.29208	-0.20471	-0.26198	0.076151	0.019251	0.2092021	0.2284527	0.053145	0.0881423	0.239467	0.3807545	0.074671	0.0612974	0.1412511	0.2558363	0.5330562	0.00556	0.192	0.030212	0.1940229	0.263563	0.685358		
5/8	1.9635	-23	-0.38268	-0.27144	-0.34612	0.07352	0.0323	0.1882597	0.22056	0.028888	0.13785	0.2008622	0.3676	0.096899	0.0118108	0.2059091	0.200021	0.51464	0.004271	0.2016121	9.511E-05	0.2636316	0.1920697	0.66168		
21/32	2.06167	-28	-0.4714	-0.33669	-0.42756	0.070181	0.046786	0.1637574	0.2105432	0.009749	0.1819466	0.15921	0.3509053	0.097378	0.0017678	0.2476519	0.1444697	0.4912675	0.037074	0.1423665	0.0368474	0.2889299	0.1264122	0.6316296		
11/16	2.15984	-34	-0.55557	-0.40075	-0.50566	0.066166	0.061268	0.1372305	0.1984987	0.000453	0.2117866	0.0185914	0.3308312	0.07584	0.0354425	0.2562296	0.0956517	0.4631637	0.007074	0.0595976	0.119808	0.2657133	0.074394	0.5954962		
23/32	2.25802	-39	-0.63439	-0.46272	-0.57981	0.061514	0.07427	0.1102726	0.1845427	0.003306	0.2218986	0.028366	0.3075711	0.042267	0.0988717	0.2320403	0.0574203	0.4305995	0.100276	0.0027811	0.2039892	0.2079818	0.0386002	0.553628		
3/4	2.35619	-45	-0.70711	-0.5225	-0.64945	0.05627	0.084405	0.0844047	0.1688093	0.017584	0.2110116	0.0527529	0.2813488	0.012309	0.1661717	0.1846352	0.0307725	0.3938884	0.08358	0.0197823	0.2472793	0.1384764	0.0173095	0.5064279		
25/32	2.45437	-51	-0.77301	-0.57981	-0.71401	0.050483	0.090498	0.0609519	0.1514502	0.039647	0.1821075	0.030663	0.2524171	7.95E-06	0.2107211	0.1282576	0.0143972	0.3533839	0.041894	0.0955418	0.2329693	0.0774268	0.0065185	0.4543507		
13/16	2.55254	-56	-0.83147	-0.63439	-0.77301	0.044211	0.091694	0.0409382	0.1326326	0.063748	0.1415113	0.0157949	0.2210544	0.011157	0.216194	0.0764376	0.0056878	0.3094761	0.006366	0.179544	0.1746234	0.0353896	0.001975	0.3978979		
27/32	2.65072	-62	-0.88192	-0.68598	-0.82598	0.037513	0.08753	0.0250075	0.1125377	0.083364	0.0972525	0.0069463	0.1875628	0.040346	0.1826215	0.0378192	0.0018008	0.2625879	0.003719	0.2179268	0.1029107	0.012606	0.0004502	0.337613		
7/8	2.74889	-68	-0.92388	-0.73432	-0.8725	0.030453	0.07798	0.0133792	0.0913589	0.092716	0.0570993	0.024492	0.1522649	0.07311	0.1250088	0.0146335	0.0004185	0.2131709	0.035836	0.1894957	0.0454616	0.0032145	6.894E-05	0.2740768		
29/32	2.84707	-73	-0.95694	-0.7792	-0.91221	0.0231	0.063461	0.0058396	0.0693004	0.088148	0.0267377	0.0006151	0.1155006	0.092259	0.0654389	0.0039428	6.047E-05	0.1617008	0.077294	0.1166004	0.0135027	0.0004984	5.732E-06	0.2079011		
15/16	2.94524	-79	-0.98079	-0.8204	-0.94481	0.015525	0.044802	0.0017726	0.0465744	0.069014	0.0085258	8.433E-05	0.077624	0.08559	0.0225117	0.0005679	3.745E-06	0.1086736	0.093044	0.0445675	0.0020793	3.242E-05	1.603E-07	0.1397232		
31/32	3.04342	-84	-0.99518	-0.85773	-0.97003	0.0078	0.023175	0.0002248	0.0233999	0.037884	0.0011133	2.7E-06	0.0389998	0.051509	0.0030722	1.872E-05	3.026E-08	0.0545997	0.063671	0.00664568	7.127E-05	2.697E-07	3.271E-10	0.0701996		
1	3.14159	-90	-1	-0.89101	-0.98769	9.75E-18	2.92E-17	4.39E-49	2.925E-17	4.87E-17	2.195E-48	8.237E-81	4.875E-17	6.82E-17	6.146E-48	5.766E-80	1.44E-112	6.825E-17	8.77E-17	1.317E-47	2.224E-79	1.3E-111	2.44E-144	8.774E-17		



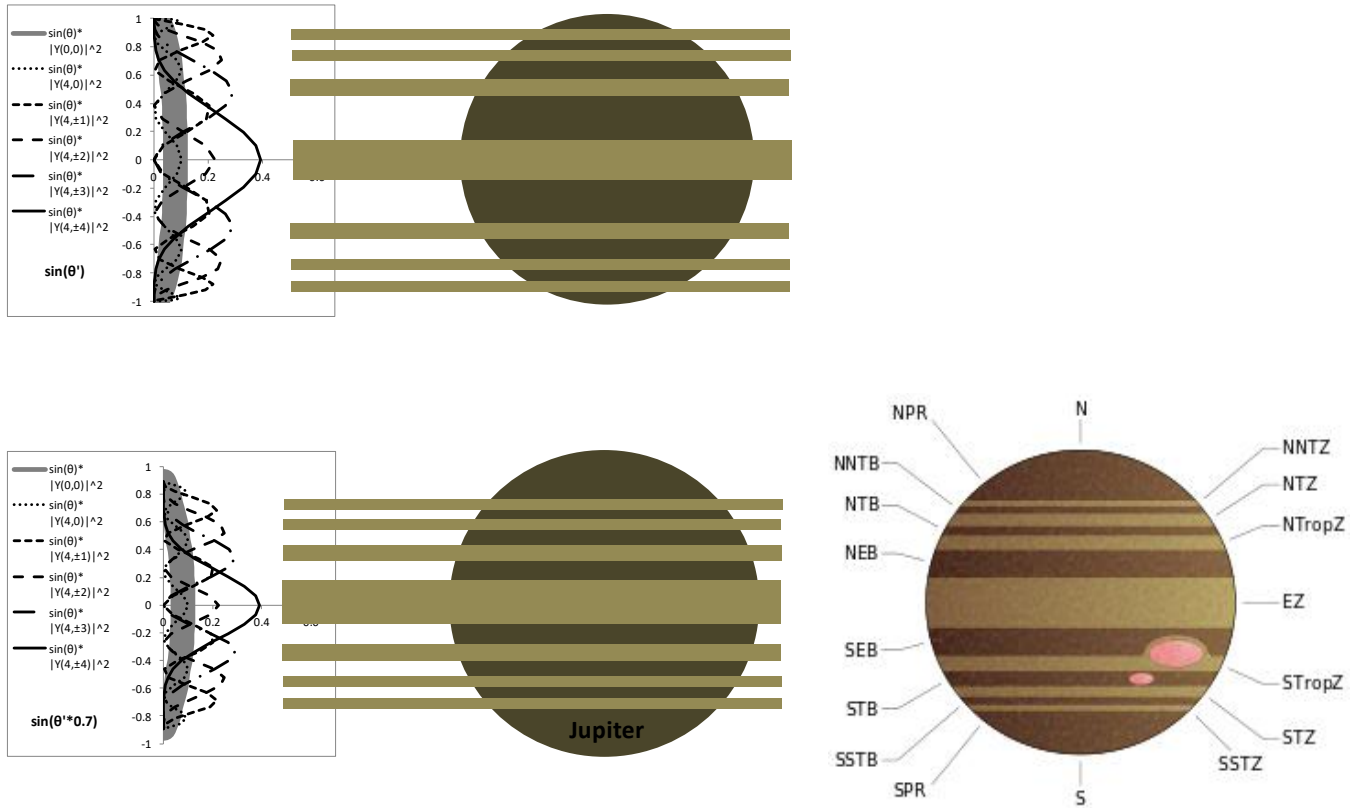


Figure 3a (top). Transforming Figure 2b into a Figure 3c -like plot, by switching the x and y in the plot, and extending (the band) of peaks to the front of a ball that pretend to be Jupiter.

Figure 3b (bottom-left & middle). Transforming Figure 2c into a Figure 3c -like plot, by switching the x and y in the plot, and extending (the band) of peaks to the front of a ball that pretend to be Jupiter.

Figure 3c (bottom-right). Idealized illustration of Jupiter's cloud bands, copied from wiki "Atmosphere of Jupiter" [3].

Figure 3c shows an idealized illustration of Jupiter's cloud bands (obtained from wiki "Atmosphere of Jupiter"). I believe that the seven cloud bands in Figure 3c are actually come from the 7 probability peaks in Jupiter's $n = 5, l = 4$ subshells in Figure 2a. To get a more direct visual comparison, I need to transform Figure 2a plot into Figure 3c kind of plot. Figure 2a is the original $\sin(\theta) * |Y(4,m)|^2$ (and $\sin(\theta) * |Y(0,0)|^2$) vs. θ' plot. When we view a 3D spherical surface in a 2D plan, θ' need to be projected as $\sin(\theta')$ (see in Figure 2b). Then in Figure 3a, I transformed Figure 2b into a Figure 3c -like plot, by switching the x-axis and y-axis in the plot, and extending (the band) of peaks to the front of a ball that pretend to be Jupiter. Although comparable to Figure 3c, the 7 bands in Figure 3a are too separated from each other. We know that the spin of Jupiter generates the equator-toward force (from both the centrifugal force and the Coriolis force). This equator-toward force will move all 7 bands more closer to the equator. So in Figure 2c I mimic this effect by simply multiplying a factor of 0.7 to the θ' . (Again, there may be a more accurate way to do it, but I do not know since I am only the citizen level QM scientist). Then in Figure 3b, I transformed Figure 2c into a Figure 3c like plot. So now they become almost same.

A detailed analysis shows that the $\sin(\theta) * |Y(4,4)|^2$ peak forms the major band at equator, the two peaks of $\sin(\theta) * |Y(4,3)|^2$ forms a band on each side of equator, the two peaks of $\sin(\theta) * |Y(4,2)|^2$ forms a (further away) band on each side of equator, the two peaks of $\sin(\theta) * |Y(4,1)|^2$ forms a band near two (north or south) poles, and the background of Jupiter's surface is represented by the $\sin(\theta) * |Y(0,0)|^2$ probability density. So at least apparently, the pattern of Jupiter's 7 major cloud bands can be mimicked by the 7 major peaks of the $\sin(\theta) * |Y(4,m(=4,3,2,1))|^2$ probability density. In 3D, these 7 major peaks of the $\sin(\theta) * |Y(4,m(=4,3,2,1))|^2$ probability density forms 7 rings on top of the $|400\rangle$ state shell surface. We know that $m = 0$ means there is no m layer differentiation in θ -dimension, so for $|400\rangle$ state shell it has a homogeneous mass

density sphere. Since $|400\rangle$ shell is formed of gas, it has a soft surface. So we can think that the 7 mass peak rings of $|54m\rangle$ are embed on the surface of the soft $|400\rangle$ shell (see Figure 4).

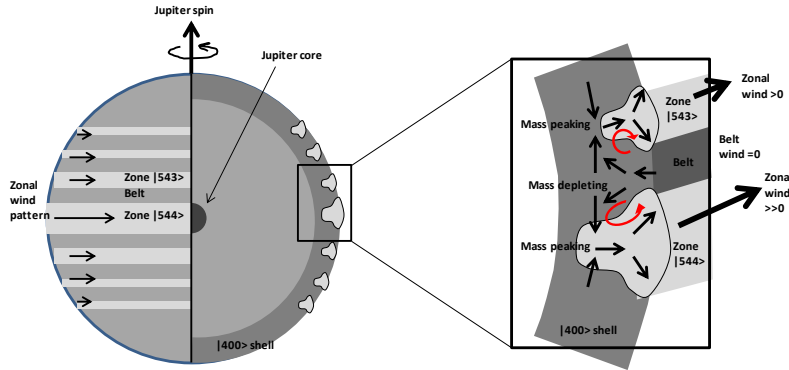


Figure 4. Illustration of how the QM mass peaking/depleting effect produces Jupiter surface's zone/belt bands.

Now let us add the dynamic physics meaning on to it: at the peaks of the $\sin(\theta) * |Y(4,m(=4,3,2,1))|^2$, the QM effect causes the mass density (of gas) significantly higher than the nearby θ' positions, but according to the second law of thermodynamics, the mass density in θ -dimension has the tendency to get even everywhere for the purpose of maximizing its entropy. To do that, this high mass density region will have to expend its volume.

Let us consider a small unit volume (r to $r + dr$, θ to $\theta + d\theta$, and ϕ to $\phi + d\phi$) in the sub-shell of $R(5,4)$, which can be further simplified as a small cube with 6 faces, and it is in the mass density $\sin(\theta) * |Y(4,m(=4,3,2,1))|^2$ peak region in θ -dimension. It needs to expend the volume to release the pressure of high mass density. At the face close to the center of Jupiter, the mass density is even higher due the stronger gravity generated mass density, so it cannot expend in $-r$ direction. At the two faces in ϕ -dimension, the mass density is the same as that in the θ -dimension's peak region, so it cannot expend in ϕ directions. At the two faces in θ -dimension, the mass density is lower, but a QM force maintains this density difference, so it cannot expend in θ directions. Only at the face away from Jupiter's center, the mass density is lower, and it is free to expend its volume in $+r$ direction.

The outward expending of $\sin(\theta) * |Y(4,m(=4,3,2,1))|^2$'s peaks caused by QM moves the mass (or gas) from underneath the surface to Jupiter's surface. The ϕ degeneracy make these θ -dimension peaks form ring-band in ϕ -dimension on the Jupiter's surface. So the upwelling $\sin(\theta) * |Y(4,m(=4,3,2,1))|^2$ peaks forms bands on Jupiter's surface and called zones, and the background $|Y(0,0)|^2$ become belts. The same QM mass peaking effect causes the mass depleting effect in (belt) region between two mass peaks, so while the mass in zones keeps (actively) upwelling (driven by QM's mass peaking effect), the mass in belts has to keep (passively) down welling (driven by the QM's mass depleting effect). Therefore, it forms the convection between zones and belts on Jupiter surface (see Figure 4 right).

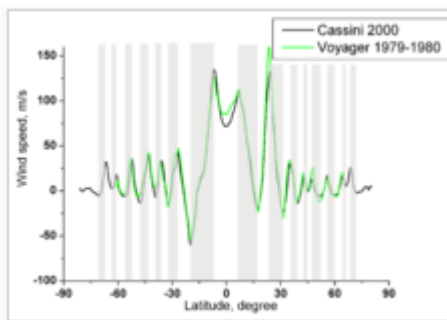


Figure 5. Zonal wind speeds in the atmosphere of Jupiter, copied from wiki "Atmosphere of Jupiter" [4].

Figure 5 shows that in general all zonal bands have eastward wind and the belt bands have zero (or westward) wind. According to my previous study result in paper SunQM-3s1 section I-b, a spinning Sun (and Jupiter) has its inner shell's spin velocity faster than that of the outer shell. So the inner sub-shell of $\sin(\theta) * |Y(4, m(=4, 3, 2, 1))|^2$'s 7-peaks carried their faster v_{spin} to the surface and forms 7 major fast moving cloud (zone) band on Jupiter's surface. (Note: here we need to use the multiplier n' sub-shell concept, e.g. $|544\rangle$ state can have an inner sub-shell $n' = 3094$, and an outer sub-shell $n' = 3125$, see Table 3 for detailed explanation). The outer sub-shell of $\sin(\theta) * |Y(0, 0)|^2$ (which has a slower v_{spin}) left as the background on Jupiter's surface and it becomes slow moving cloud (belt) bands.

If this model is correct, then all zones will have eastward wind, and all belts will have zero wind (because $|Y(0, 0)|^2$ spins with Jupiter at same v_{spin}). But then where are those westward wind (in belts, see Figure 5) come from? Remember that the 7 zone bands come from the 7 peaks of $\sin(\theta) * |Y(4, m(=4, 3, 2, 1))|^2$? Actually in the complete $\sin(\theta) * |Y(4, m(=4, 3, 2, 1))|^2$, there are two sets of $m(s)$, one with $m = +4, +3, +2, +1$, and they have (averaged) eastward moving mode. Since these modes moving in the same direction as Jupiter's spin direction, its Coriolis force pushed them toward to the equator. Another one with $m = -4, -3, -2, -1$, and they have (averaged) westward moving mode. Since these modes moving in the opposite direction as Jupiter's spin direction, its Coriolis force pushed them away from the equator. Or the negative m has θ' phase shifted from the positive m in θ -dimension. This phase shift causes each $+m$ (and eastward wind) band (=zone) unpairing with its $-m$ (and westward wind) band (=belt) at the non-equator region. And this makes the speed plot of $+/-m$ pair (or zone/belt pair) in Figure 5 like a 1st order differentiation curve. (Note: if there is no phase shift, the $+m$ model will completely suppress the $-m$ model). So now with QM theory, we can qualitatively explain the (eastward/westward) wind pattern in Jupiter atmosphere's zone/belt bands.

In this model, the out most shell is simplified into only two sub-shells, $|544\rangle$ and $|400\rangle$. In a more realistic (also more complicated) model, other states (like $|41m\rangle$, $|42m\rangle$, $|43m\rangle$, $|54m(=0, 1, 2, 3)\rangle$ see Figure 1a) also make small contribution to Jupiter's surface QM. These many small contributors are expected to modulate the 7 major peaks to generate more minor zones and belts.

In this way I discovered a QM theory for the cloud bands on Jupiter surface: they originated from the QM mass peaking/depleting effect in Jupiter's $\{N, n\}$ QM structure. My explanation for Jupiter's cloud bands is very different from the current popular "Hadley cell" -type explanation. In the Hadley cell theory, the upwelling of the mass (in zone) is due to its lower mass density caused by the higher temperature. In my theory, the upwelling of the mass (in zone) is due to its higher mass density caused by the QM's mass peaking effect. Wiki "Atmosphere of Jupiter" mentioned that "*Zones, which are colder than belts, correspond to upwellings, while belts mark descending air*", it clearly favors my theory than the "Hadley cell" -type theory because the zone region is not warmer. I believe that after accurately measured the mass density and temperature in zones and belts, my theory will be proved to be correct.

I-b. Using interior $\{N, n\}$ QM to calculate out the depth of the mass peak origin of Jupiter cloud bands

If we know the quantitative relationship of the spin velocity at each (multiplier n') sub-shell, then we can calculate out the depth of the mass peak origin of Jupiter cloud bands (solely) from the (mass) probability density $r^2 * |R(5, 4)|^2 * |Y(4, m)|^2 * \sin(\theta)$. Now let us try it. Suppose Jupiter atmosphere's wind speed is in a spin frame of $\omega_{n-spin} = \omega_{1-spin} / n^x$, where $x \approx 3$ (see paper SunQM-3s1 section I-b), then Jupiter atmosphere's wind speed has a relationship $v_{n-spin} = v_{1-spin} / n$, and $r_n = r_1 * n^2$. We still use the simplest model: on Jupiter surface, all zonal bands are caused by $|54m\rangle$ QM state, and all (background) belt bands are caused by the $|400\rangle$ state. From Figure 5, we see that $m = +4, +3, +2, +1$ zonal bands (in latitude $0 \sim -90^\circ$) have eastward wind with speed at 125, 40, 30, and 35 m/s relative to the background's zero speed. $|Y(0, 0)|^2$ sub-shell should have the zero speed (relative to the background speed), which means it has the same v_{spin} as the Jupiter surface's whole background's v_{spin} . Now let us determine the Jupiter surface whole background's v_{spin} .

From wiki "Rotation period", Jupiter rotation period at equator is 0.41007 days = 35430 s, $v_{spin} = 2\pi r_{Jupiter} / \text{period} = 2\pi * 71492,000 \text{ m} / 35430 \text{ s} = 12678 \text{ m/s}$. Jupiter rotation period at high latitude is 0.41369942 days = 35743 s, $v_{spin} = 2\pi * 71492,000 \text{ m} / 35743 \text{ s} = 12567 \text{ m/s}$. So this calculation shows that Jupiter equator's eastward wind speed is 111 m/s faster than the high latitude's eastward wind speed, which is practically the same as from Figure 5's 125 m/s. Therefore we can choose Jupiter high latitude's eastward wind speed (=12567 m/s) as the Jupiter surface whole background's v_{spin} .

In Table 3, I use the interior $p\{N,n\}$ QM structure to calculate the depth of mass peaks: the outer (multiplier n') sub-shell of $|544\rangle$ and $|400\rangle$ at surface $p\{-1,5\}$ has $v_{1-spin} = 12567$ m/s. The inner (multiplier n') sub-shell of $|544\rangle$ is at the v_{n-spin} . Then $n = v_{1-spin} / v_{n-spin}$. The resulted n is less than 1 because of the interior $\{N,n\}$. Then $r_n = r_1 * n^2$, with $r_1=7.1492E+7$ meters. Finally, $Depth = r_1 - r_n$. In columns 4 to 6, I use the base-frequency n (therefore non-integer) and interior QM to calculate the depth. In columns 7 to 10, I use the high-frequency multiplier n' (therefore almost integer) and a mixture of exterior/interior QM to calculate the depth.

Table 3, Using the interior $\{N,n\}$ QM structure to calculate the depth of mass peaks of $|54m\rangle$ QM states near the surface of Jupiter.

	relative v_{n-spin} from Fig. 3	absolute v_{n-spin} m/s	$n = v_{1-spin} / v_{n-spin}$	$r_n = r_1 * n^2$	Depth= $r_1 - r_n$	$n' = v_{n'+1} / v_{n'}$ $(v_{n'} - v_{n'+1})$	$n'' = v_{n''+x} / v_{n''}$ $*(n''+x) =$	$r_{n''} = r_{n''+x} * n''^2$ $/(n''+x)^2$	Depth= $r_{n''+x} - r_{n''}$
	m/s	m/s		m	m			m	m
-7°, m=+4	125	12692	0.9902	7.009E+07	1.40E+06	100.5	3094.2	7.009E+07	1.40E+06
-25°, m=+3	40	12607	0.9968	7.104E+07	4.53E+05	314.2	3115.1	7.104E+07	4.53E+05
-36°, m=+2	30	12597	0.9976	7.115E+07	3.40E+05	418.9	3117.6	7.115E+07	3.40E+05
-42°, m=+1	35	12602	0.9972	7.110E+07	3.97E+05	359.1	3116.3	7.110E+07	3.97E+05
-51°	30	12597	0.9976	7.115E+07	3.40E+05	418.9	3117.6	7.115E+07	3.40E+05
-60°	15	12582	0.9988	7.132E+07	1.70E+05	837.8	3121.3	7.132E+07	1.70E+05
-67°	30	12597	0.9976	7.115E+07	3.40E+05	418.9	3117.6	7.115E+07	3.40E+05
$ Y(0,0) ^2$	0	12567	1	7.149E+07	0.00E+00		3125	7.149E+07	0.00E+00

Note: data of relative v_{n-spin} and θ' was estimated from Figure 5.

The result (in column 6) shows that a mass density peak of $|Y(4,4)|^2$ at 1400 km below the surface of Jupiter keep uprising to the surface and forms a zonal cloud band at equator, and this band has eastward wind ~125 m/s faster than the whole surface background's v_{spin} . It also shows that a mass density peak of $|Y(4,3)|^2$ at 453 km below the surface of Jupiter keep uprising to the surface and forms a zonal cloud band at about -25° latitude, and this band has eastward wind ~40 m/s faster than the whole surface background's v_{spin} . And same for $m = +2$ and $m = +1$ bands.

Besides the non-integer interior n calculation method, I can also use the high-frequency multiplier (integer) n' for the same calculation (as shown in columns 7- 10 in Table 3): To do that, let us first estimate the minimum n' value under the condition that if we assume $\Delta n' = 1$ between the inner sub-shell $v_{n'}$ and the most out sub-shell $v_{n'+1}$. Using $v_1 = v_{n'} * n' = v_{n'+1} * (n'+1)$, we obtain $n' = v_{n'+1} / (v_{n'} - v_{n'+1})$, here $v_{n'+1} = 12567$ m/s. So column 7 of Table 3 shows the minimum n' for each zone's $v_{n'}$. They are between 101 to 838. Now let us find a common (minimum) n' that can fit for all of them. For $|54m\rangle$ state, the multiplier n'' of $n = 5$ are: $n'' = 5 * 5 = 25$, $5 * 5^2 = 125$, $5 * 5^3 = 625$, $5 * 5^4 = 3125$, etc. The initially estimated results in column 7 make me to choose 3125 as the minimum common n'' . It is easier to use the interior $\{N,n\}$ QM, so I choose the multiplier $(n''+x) = 3125$ for Jupiter surface. Then the other inner sub-shell's (interior) multiplier $n'' = v_{n''+x} / v_{n''} * (n''+x)$, and results are listed in column 8. Then we can calculate the $r_{n''}$ by $r_{n''} / n''^2 = r_{n''+x} / (n''+x)^2 = r_1$, or $r_{n''} = r_{n''+x} * n''^2 / (n''+x)^2$. The results are shown in column 9. The final depth is listed in column 10. We can see that the result of column 10 is the same as that in column 6 (as expected).

The advantage of using this (exterior) calculation is that now we know the n'' value for each n'' sub-shell, so we can use a complete QM language to explain the forming of Jupiter's cloud bands: For $|544\rangle$ state, the QM-force peaks the mass (gas) density in θ -dimension at around equator (zonal) region in $n = 5$ shell's multiplier $n''=3094$ sub-shell (with $r = 7.01E+7$ m), This increases the pressure of the local mass (or gas), and excites the mass from (the low energy) $n'' = 3094$ state to higher energy $n'' = 3125$ state (by moving it from $r = 7.01E+7$ m orbit to $7.15E+7$ m orbit). It forms the (uprising) zone on Jupiter surface. There, the QM peaking force in θ -dimension is gone, so mass diffuses in θ -dimension to the neighboring belt region (driven by entropy), and then further de-excited back to $n'' = 3094$ state in belt region (driven by G-force). Then the QM depleting force will move the mass from the $n'' = 3094$ belt region to the $n''=3094$ zone region again to peak the local mass density (so that it forms a complete convectional cycle). The same explanation is valid for other zonal bands formed by states of $|543\rangle$, $|542\rangle$, etc. Here we see again that the QM character is determined not only by the base-frequency n , but also by the high-frequency multiplier n'' .

The result shows that in general the major zonal band has a deeper origin from the surface, and the minor zonal bands have a shallow origin from the surface. Wiki "Atmosphere of Jupiter" mentioned that (Jupiter) scientists are looking for the combination of "shallow model" and "deep model", and I believe that my theory matches what they are looking for.

I-c. Demonstration of a complete radial probability density distribution from Jupiter's inner core at $p\{-2,1\}$ to its moons at $p\{0,n=1..5\}$

In Figure 6, for $r/r_1 \leq 1$, it is Jupiter's body, it has ~100% mass occupancy, so all states of $|nlm\rangle$ are fully filled with mass. For $p\{-2,n=1..4\}$ o super-shell, I plot the sum of $r^2 * |R(n,l)|^2$ for $\Sigma n = 1..4$. For $p\{-1,n=1..4\}$ o super-shell, I plot the sum of $r^2 * |R(n,l)|^2$ for $\Sigma n = 1..4$, plus $r^2 * |R(5,4)|^2$, and r/r_1 is compressed at ≥ 1 . For $r/r_1 > 1$, in general it has < 1% mass occupancy, so almost all mass falls into the nLL state. Therefore I plot only $r^2 * |R(n,L)|^2$. The four probability density curves of $|R(2,1)|^2$, $|R(3,2)|^2$, $|R(4,3)|^2$, $|R(5,4)|^2$ come from the four major moons of Jupiter: Io, Europa, Ganymede, and Callisto. The maximum mass probability of these four moons orbits are at $r/r_1 = 2^2, 3^2, 4^2$, and 5^2 (as expected). A prediction of Jupiter's internal mass density vs. r (calculated from $\{N,n\}$ QM probability function) will be given in paper SunQM-3s6.

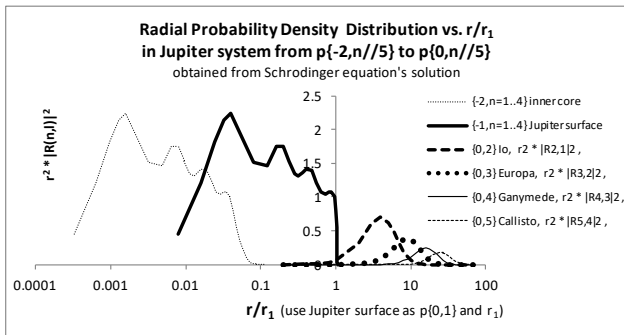


Figure 6. Radial Probability density distribution for the Jupiter system from Jupiter's inner core in $p\{-2,n\}$ super-shell to its moons in $p\{0,n=2..5\}$ super-shell. Note: it uses Jupiter' surface as $p\{0,1\}$ and as r_1 . The intensities of $r^2 * |R(n,l)|^2$ in Figure are not on scale.

II. Estimate Saturn's $|nlm\rangle$ state for its surface atmosphere band pattern

From my analysis in paper SunQM-1s3 section X, the current Saturn has a Earth-sized core $p\{0,1/2\}$ and a inner core $p\{-1,1/2\}$, both with 100% mass occupancy. But it has a $p\{0,3/2\}$ sized atmosphere. The atmosphere from $p\{0,1/2\}$ to $p\{0,2/2\}$ has 100% mass occupancy. But the atmosphere from $p\{0,2/2\}$ to $p\{0,3/2\}$ has probably only ~50% mass occupancy. I believe that if Saturn had 100% mass occupancy in atmosphere shell between $p\{0,2/2\}$ and $p\{0,3/2\}$, it would have generated enough G-forced compression to transform its core from $\{N,1/2\}$ QM to $\{N,1/3\}$ QM, so that the whole Saturn would become a $\{N,n/3\}$ QM structure. However, current Saturn's ~50% mass occupancy in $n = 3$ shell is not enough to make this transformation, so it is trapped at this hybridized (core is base-2, atmosphere is base-3) QM state. For this reason, it is better to choose Saturn's Earth-sized core (not the Saturn's surface) as the $p\{0,1\}$.

If this is correct, then the out most n shell of Saturn is $n = 2$ orbit (though ends at $n = 3$). Based on the analysis of Jupiter's atmosphere, we know that at $r/r_1 = 9$, there should be a thin (compressed) shell of $|32m\rangle$ state. Underneath it is a shell of $|200\rangle$ state. Therefore, Saturn surface's zonal bands should be dominated by $|Y(2m)\rangle^2$ peaks, with $|Y(22)\rangle^2$ peak at the equator, and $|Y(21)\rangle^2$ peaks at both side of $\theta' \approx \pm \pi/4$ (shown in Figure 7a, 7b, 7c). Here I use the same spin caused scaling factor ($= 0.7$ for $y = \sin(\theta' * 0.7)$) as that for Jupiter. Considering Saturn has the similar radius and spin speed ($r = 5.82E+7$ m, 10.7 hours/day) as that of Jupiter ($r = 6.99E+7$ m, 9.9 hours/day), the same $\theta' * 0.7$ scaling factor is expected. The

observed atmosphere band pattern of Saturn (from either wiki "Saturn" or wiki "Planetary core", see Figure 7c) matches a $|322\rangle$ QM surface pattern (see Figure 7b). So the cloud band pattern on Saturn surface must also originated from the QM mass peaking/depleting effect in Saturn's $\{N,n\}$ QM structure. Once Cassini's data opens, we may have the relative speed of zonal wind on Saturn surface. From it we will be able to estimate how deep this convection starts.

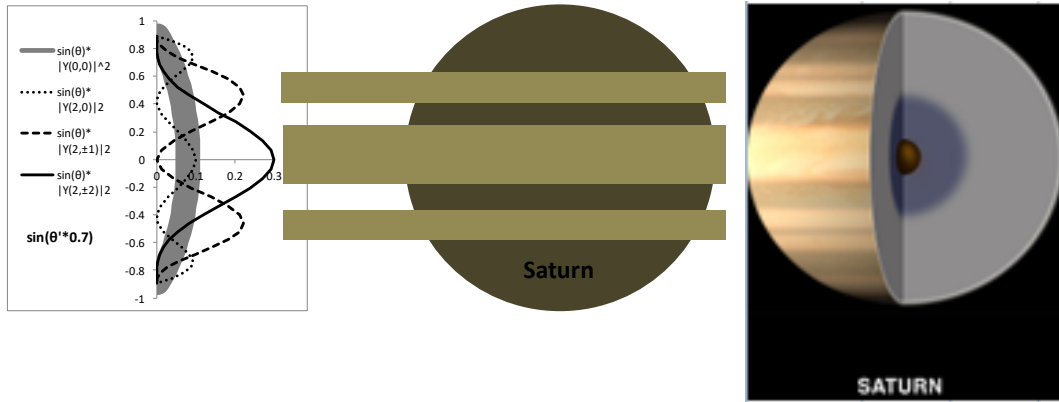


Figure 7a (left). Plot of $\sin(\theta)*|Y(2,m)|^2$ (and $\sin(\theta)*|Y(0,0)|^2$) vs. $\sin(\theta' *0.7)$.

Figure 7b (middle). Simplified Figure 7c by expending (the band) of peaks to the front of a ball that pretends to be Saturn.

Figure 7c. Saturn's atmosphere cloud bands (copied from wiki "Planetary core" ^[5]). Saturn surface $|nlm\rangle$ state analyzed as $|32m\rangle$.

III. Schrodinger equation and solution for Earth: surface atmosphere bands and the body construction

If the cloud bands on Jupiter can be explained with the QM mass peaking/depleting theory, then the atmosphere circulation pattern on Earth have to be explained with the same theory. In this section, I will use the $R(nl)Y(lm)$ wave function from the Schrodinger equation solution to construct a complete Earth body plus its atmosphere, then use the same QM mass peaking/depleting theory to explain the atmosphere circulation on Earth.

III-a. Using Schrodinger equation and solution to explain the atmosphere circulation pattern on Earth

Figure 9c shows an idealized view of three large circulation cells in Earth's atmosphere. From paper SunQM-1s3, we know that Earth can be described by a $p\{N,n/2\}$ QM structure, which means its moon's orbits can be described by the exterior $p\{N,n/2\}$ QM, and its internal structure (mainly the inner core) can be described by the interior $p\{N,n/2\}$ QM. Earth atmosphere locates just outside the surface. So it is Earth's exterior $p\{N,n\}$ QM structure if we use the surface as $p\{0,1\}$.

Now let us build a detailed Earth's $p\{N,n/2\}$ QM model (including atmosphere) for Schrodinger equation: For a $p\{N,n/2\}$ QM system, according to the rule of "all mass between r_n and r_{n+1} belong to orbit n (see paper SunQM-3s2)", each of its N super-shell contains only $n = 1$ orbit shell.

First, let us use only the base-frequency n for analysis. Earth main body (including mantle and outer core) mass is in $p\{-1,1\}$ orbit, and this orbit covers shell space from $p\{-1,1\}$ to $p\{-1,2\} = p\{0,1\}$. Earth inner core mass is in $p\{-2,1\}$ orbit, and this orbit covers shell space from $p\{-2,1\}$ to $p\{-2,2\} = p\{-1,1\}$. Earth atmosphere is in $p\{0,1\}$ orbit, and this orbit covers shell space from $p\{0,1\}$ to $p\{0,2\} = p\{1,1\}$. So Earth atmosphere has $n = 1$ or $|100\rangle$ state, which means its mass has to be homogeneous distributed in $\theta\phi$ -2D-dimension (proportional to $|Y(00)|^2$). Because Earth atmosphere is believed to have $< 1\%$ mass occupancy, it cannot occupy all orbit space between $p\{0,1\}$ and $p\{1,1\}$, so the mass only stay at $p\{0,1\}$ end region.

This is the $p\{N, n/2\}$ QM explanation of why beneath the Earth surface $p\{0, 1\}$ is a solid Earth ball, and above the Earth surface $p\{0, 1\}$ is a thin layer of (almost homogeneous) atmosphere. After Earth spinning, the atmosphere flattens at the equator as shown in Figure 9c. So by using the base-frequency n , we can perfectly explain the Earth ball and atmosphere in $p\{N, n/2\}$ QM structure, although we still cannot explain the atmospheric circulation.

Second, to explain the Earth's atmospheric circulation, we need to use the high-frequency multiplier n' $p\{N, n\}$ QM. Earth atmosphere's orbit $p\{0, 1/2\}$ has $n = 1$. Its multiplier $n' = 1 \cdot 2^1 = 2, 1 \cdot 2^2 = 4, 1 \cdot 2^3 = 8, \text{etc.}$ After some tries, I find $n' = 2$ can be used for the explanation. From my previous paper SunQM-2, we know that the increased n' value means the chosen r_1 is moved inward. So when we use $p\{N, n/2\}$ QM at $n' = 2$, it means we define Earth's inner core $p\{-1, 1\}$ as r_1 . Therefore from Earth inner core to Earth surface is $n = 1$ orbit shell, and the atmosphere locates at $n = 2$ orbit shell. The $n = 2$ shell is further composed by two sub-shells, $|21m\rangle$ at inner, and $|200\rangle$ at outer in r -dimension. Because Earth atmosphere is believed to have $< 1\%$ mass occupancy, due to the spin induced nLL effect, all atmosphere mass can be simplified to stay at $|21m\rangle$ state, while $|200\rangle$ can be simplified as a empty orbit. Solving the Schrodinger equation for $|21m\rangle$ state gives the mass density distribution $|R(2, 1)|^2 \cdot |Y(1, m)|^2$.

Now let us plot the radial probability density distribution $|R(2, l=0, 1)|^2$ along r/r_1 (see Figure 8a, 8b below).

Table 4. $r^2 \cdot |R(n, l)|^2$ vs. r/r_1 for $n = 1$ to 2.

$p\{-1, 1\}$ Earth factor r cut-off=				$p\{-1, 2\}$ Earth atmosphere
				10 4
$r_1 =$	0.160 E+7 meters			
$r/r_1 =$	$r^2 \cdot R_{1,0} ^2, \{-1, 1\}$	$r^2 \cdot R_{2,0} ^2, \{-1, 2\}$	$r^2 \cdot R_{2,1} ^2, \{-1, 2\}$	$r^2 \cdot R_{2,1} ^2, \{1, 2\}$
0.1	0.2047	0.0255	0.0000	0.1 0
0.2	0.6703	0.0829	0.0003	0.2 0
0.3	1.2348	0.1505	0.0016	0.3 0
0.4	1.7973	0.2145	0.0045	0.4 0
0.6	2.7107	0.3025	0.0185	0.6 0
0.8	3.2303	0.3235	0.0479	0.8 0
0.95	3.3746	0.3006	0.0820	0.95 0
1	3.3834	0.2874	0.0958	1 0
1.1	3.3518	0.2549	0.1269	1.1 0
1.2	3.2658	0.2169	0.1626	1.2 0
1.4	2.9797	0.1359	0.2467	1.4 0
1.7	2.4112	0.0371	0.3973	1.7 0
2	1.8316	0.0000	0.5639	2 0
2.5	1.0528	0.1002	0.8350	2.5 0
3	0.5577	0.3501	1.0502	3 0
3.5	0.2793	0.6502	1.1801	4 0
4	0.1342	0.9158	1.2210	4 1.2210
4.5	0.0625	1.0984	1.1863	4.07 1.1863
5	0.0284	1.1844	1.0967	4.10 1.0967
5.5	0.0126	1.1831	0.9739	4.12 0.9739
6	0.0055	1.1154	0.8366	4.13 0.8366
7	0.0010	0.8727	0.5702	4.15 0.5702
8	0.0002	0.6038	0.3578	4.16 0.3578
9	0.0000	0.3827	0.2109	4.17 0.2109
10	0.0000	0.2270	0.1182	4.18 0.1182
12	0.0000	0.0691	0.0332	4.19 0.0332
14	0.0000	0.0183	0.0083	4.20 0.0083

Note: use Earth inner core $p\{-1, 1/2\}$ as r_1 , which is $1/4$ of Earth surface $p\{0, 1/2\}$'s r , $r_1 = 6.378E+6 / 4 = 0.160E+7$ m.

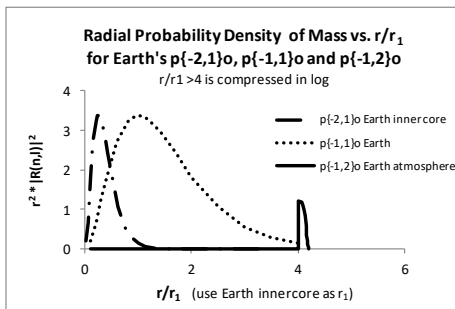
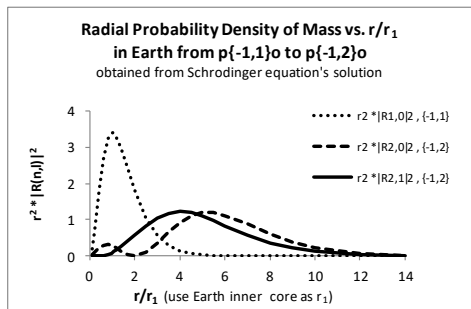


Figure 8a (left). The original $r^2 * |R(n,l)|^2$ vs. r/r_1 plot for Earth's $p\{-1,1\}$ and $p\{-1,2\}$ orbit shells in r-dimension. Figure 8b (right). Radial Probability Density of Mass vs. r/r_1 for Earth's $p\{-2,1\}$, $p\{-1,1\}$ and $p\{-1,2\}$ orbit shells with border at $r/r_1 = 4$. The intensities of $r^2 * |R(n,l)|^2$ in Figure are not on scale.

Figure 8a shows the plot of the original radial wave function from Schrodinger equation's solution of $r^2 * |R(n,l)|^2$ vs. r/r_1 , for Earth's $p\{-1,1\}$ and $p\{-1,2\}$ orbit shells in r-dimension. Combination of these mass density distributions for Earth's orbit shells of $p\{-2,1\}$, $p\{-1,1\}$, $p\{-1,2\}$, and so on, constructed a complete Earth ball (as shown in Figure 8b). In the Figure 8b, for $p\{-1,1\}$ $n = 1$ orbit shell, a boundary condition that $r^2 * |R(1,0)|^2 = 0$ is added to $r/r_1 > 4$, to reflect the fact that outside the Earth surface, the mass density ≈ 0 . For $p\{-1,2\}$ orbit shell (where atmosphere locates), another boundary condition is added: $r/r_1 > 4$ is compressed logarithmically using $[4 * 10 + \log(r/r_1 * 10^{-4} * 10)]/10$. This cut-off let the $|21m\rangle$ state (which is atmosphere) has a maximum mass density at Earth's surface $r/r_1 = 4$, and the density decrease quickly as r/r_1 increasing. So Figure 8b shows how I constructed a complete Earth body plus its atmosphere, by using the Schrodinger equation's solution (the wave function) and Earth's $p\{N,n\}$ QM structure.

Now we can use the QM mass peaking/depleting theory to explain the circulation of Earth's atmosphere. First consider the r-dimension. Unlike that Jupiter's interior $\{N,n\}$ atmosphere (close to 100% mass occupancy), where we need to use solid shell to simplify the analysis, Earth's exterior $p\{-1,2\}$ atmosphere (< 1% mass occupancy) makes all mass in $|2,1,1\rangle$ state and stay only near Earth's surface, so we do not need the solid shell simplification. Then in $\theta\phi$ -dimensions, we only need to analyze the θ -dimension. Table 2 columns 8 & 9 shows the (original) probability density distribution of $\sin(\theta) * |Y(1,m)|^2$.

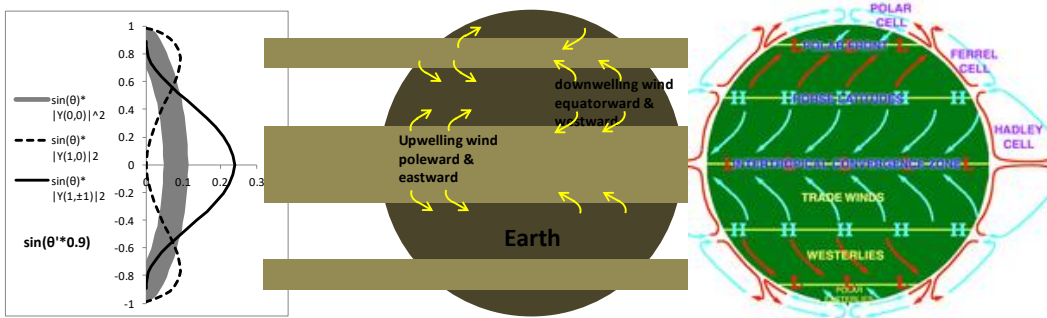


Figure 9a. Plot of $\sin(\theta) * |Y(1,m)|^2$ (and $\sin(\theta) * |Y(0,0)|^2$) vs. $\sin(\theta) * 0.9$. Figure 9b. Simplified Figure 9c by extending (the band) of peaks to the front of a ball that pretends to be Earth. Figure 9c. An idealized view of three large circulation cells in Earth's atmosphere. Copied from wiki "Atmosphere of Earth", [6].

Let us assume that after Earth's spin, ~80% mass stay in $|2,1,1\rangle$ state, ~20% mass stay in $|2,1,0\rangle$, and $|2,1,-1\rangle$ state is completely suppressed by $|2,1,1\rangle$ state. Therefore the mass is re-distributed among three states of $|2,1,m(=0,\pm 1)\rangle$ as shown in Figure 9a. Here we see three mass density peaks, one major peak at equator, and two small ones near each pole. Then in θ -dimension the equator-toward force (generated by the Earth spin's centrifugal force) will push this mass density peak towards to the equator.

To match Figure 9c's upwelling polar front at $\theta \approx 60^\circ$ latitude, I have to re-adjust the spin caused $y = \sin(\theta * 0.9)$'s scaling factor in Figure 9a to $0.9 \times$ (rather than $0.7 \times$ for Jupiter and Saturn). In comparison with Jupiter ($r = 6.99E+7$ m, 9.9 hours/day) and Saturn ($r = 5.82E+7$ m, 10.7 hours/day), Earth has a smaller r ($= 6.38E+6$ m) and slower spin (24 hours/day), so the centrifugal force on Earth's atmosphere is expected to be significantly smaller than that on Jupiter's and Saturn's. Therefore, the scaling factor is expected to be more closer to 1. (Note: In theory, with known radius, spin speed, mass

density, temperature, we should be able to calculate out the spin caused θ' scaling factor for Jupiter, Saturn and Earth. But, again I am only a citizen level QM scientist, and I have no time to figure out how to do it at this time).

Finally, in Figure 9b, we see that the QM peaking/depleting effect causes a major mass density peak at equator, two small peaks at latitude = $\pm 60^\circ$, and two mass deplete regions at latitude $\approx \pm 35^\circ$. So the mass peak causes atmosphere a major upwelling at equator and two small upwelling at $\pm 60^\circ$ latitude, the mass depletion causes two major atmosphere downwelling at $\approx \pm 35^\circ$ latitude. This fits the Earth atmosphere's Hadley cell, the Ferrel cell, and the Polar cell quite well. In this way, we can use QM peaking/depleting effect and multiplier $n' = 2$ of $p\{N, n/2\}$ QM model to explain Earth's atmosphere circulation.

Again, the major difference between QM peaking/depleting theory and Hadley cell theory for Earth atmosphere's circulation is that Hadley cell needs air to be warmed, mass density decreased, and then upwelling, while QM peaking need air to be more dense, and then upwelling. An accurate measurement of air mass density at latitude 0° , $\pm 35^\circ$, and $\pm 60^\circ$ will immediately tell which theory is more correct. If the Hadley cell theory is right, then the upwelling region should move to north when north is in summer, or move to south when south is in summer. I do not know whether this has been observed or not.

From wiki "Atmospheric circulation", for Earth's Hadley cell, "*The poleward movement of the air in the upper part of the troposphere deviates toward the east, caused by the coriolis acceleration (a manifestation of conservation of angular momentum). At the ground level however, the movement of the air toward the equator in the lower troposphere deviates toward the west, producing a wind from the east. The winds that flow to the west (from the east, easterly wind) at the ground level in the Hadley cell are called the Trade Winds*". If using my $p\{N, n/2\}$ QM model with QM mass peaking/depleting effect, plus the spin frame of $\omega_{n\text{-spin}} = \omega_{1\text{-spin}} / n^x$, where $x \approx 3$, plus the multiplier n' , then it is much easier to explain: (Similar as Jupiter's atmosphere), Earth atmosphere's wind speed is also in a spin frame of $\omega_{n\text{-spin}} \approx \omega_{1\text{-spin}} / n^3$ (see paper SunQM-3s1, but here we use multiplier n' to replace the base-frequency n), So the Earth ground (low altitude) atmosphere has faster eastward spin speed (= eastward wind), and upper atmosphere (high altitude) has lower eastward spin speed. The upwelling atmosphere at equator region carries the faster $v_{n\text{-spin}}$ (from low altitude), forms a zonal band with relative eastward wind at high altitude. There, the QM mass peaking effect is gone, so mass diffuses in θ -dimension to the neighboring belt region (or poleward), and its $v_{n\text{-spin}}$ become slower (through velocity diffusion governed by the entropy). Then the downwelling atmosphere at latitude $\pm 35^\circ$ (caused by QM depleting effect) carries the lower $v_{n\text{-spin}}$ (from the high altitude), so it become the (relatively) westward and equatorward wind at low altitude. Therefore, the Trade Winds is the macro-QM effect on Earth's atmosphere!

However, it should be pointed out that this analysis is only for the major zone band and two major belt bands near-equator region with latitude within $\Delta\theta' \approx \pm 45^\circ$. Beyond that region, the situation is more complicated. For example, for the minor mass peak at $\theta' \approx 60^\circ$, the upwelling atmosphere at the south edge of zonal band generates east-equator-ward wind (not the east pole-ward). Meanwhile, the downwelling atmosphere at the north edge of belt band generates west-pole-ward wind (not the west-equator-ward, see Figure 9b). Because this result is caused by the minor QM mass peak effect, so it is not that obvious, and probably even submerged in the observed data.

Unlike that in Jupiter where we need to find the depth of the QM peaking effect under the atmosphere surface, in Earth, the origin of the atmosphere's QM peaking effect must be at the sea level of the Earth (simply because Earth is a solid ball).

III-b. Demonstration of a complete Radial Probability density distribution for Earth system from Earth's inner core at $\{-2,1\}$ to Moon at $\{3,1\}$

The detailed radial probability density distribution for Earth from Earth's inner core at $\{-2,1\}$ to surface at $\{0,1\}$ has been shown in Figure 10. It uses $p\{-1,1\}$ as r_1 , so $r/r_1 \leq 4$ has $\sim 100\%$ mass occupancy, $r/r_1 > 4$ in general has $< 1\%$ mass occupancy. Moon's orbit is at $p\{3,1/2\}$ orbit, so I simply use $n = 1$ radial probability $r^{*2} |R(1,0)|^2$, and scale up r/r_1 by $4\times$ from $p\{-1,1\}$ to $p\{0,1\}$, and then repeat this step up to $p\{3,1\}$. A prediction of Earth's mass density vs. r (calculated from $\{N, n\}$ QM probability function) will be given in paper SunQM-3s6.

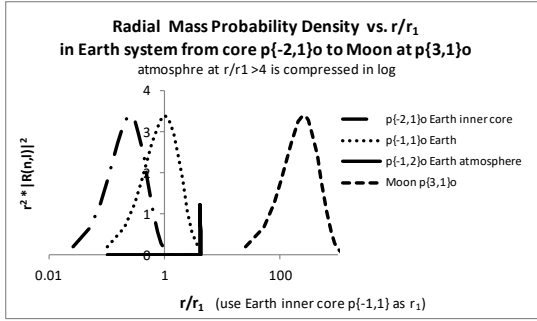


Figure 10. Demonstration of a complete Radial Probability density distribution for Earth system from Earth's inner core at $p\{-2,1\}$ to Moon at $p\{3,1\}$. Note: Intensities of $r^2 * |R(n,l)|^2$ in Figure 10 are not on scale.

IV. Using QM calculation to explain the $\{0,2//6\}$ atmosphere circulation pattern on Sun

Because Sun's surface ends at $\{0,2\}$, so I believe that it should have a $n = 2$ type atmospheric circulation pattern (like Earth's atmosphere). However, there are two major difference between Sun' $\{0,2\}$ surface layer and Earth's atmosphere:

- 1) Earth's atmosphere is out of the solid Earth surface, so it sits outside of $r/r_1 = 4$ (with Earth core $p\{-1,1//2\}$ as r_1), and it has $< 1\%$ mass occupancy, so it is quickly disappeared at above the Earth's surface. For Sun, most of its (outer shell) mass is in $|100\rangle$ state, or at $\{0,1//6\}$, or $n = 1$ orbit which starts from $\{0,1\}$ and ends at $\{0,2\}$, or from $r/r_1 = 1$ to $= 4$ using r_1 at r of $\{0,1//6\}$. At $r/r_1 = 4$, there is significant amount of $|211\rangle$ state contribution (see Figure 8a), so a thin layer of $|211\rangle$ orbit is on the surface of $r/r_1 = 4$, or embed in $|100\rangle$ shell (similar as that the Jupiter's $|544\rangle$ rings are embed in $|400\rangle$ shell)
- 2) If without hydrogen fusion, Sun's $|100\rangle$ state has only $\sim 50\%$ mass occupancy (purely from my guess). The hydrogen fusion generated thermal pressure rescales the mass occupancy from $\sim 50\%$ to $\sim 100\%$. Although spin removes the orbit energy degeneration of $|21m\rangle$ states, the heat overcome it and re-degenerates the orbit energy for $|21m\rangle$ states.

So the "big picture" of Sun surface atmospheric circulation is dominated by the embedded $|211\rangle$ state, which should cause a major (very broad) zonal band at equator with faster eastward wind, and two small zonal bands at latitude $\theta' \approx \pm 60^\circ$ (like Earth's). But then, why we do not see the zone/belt bands on Sun surface? The answer is first, due to $|211\rangle$ on top of $|100\rangle$ background, there are too fewer (and too broad) zonal bands and belt bands, and no clear interface, so it is difficult to see even for Earth's atmosphere. Second, the macro convection between $|211\rangle$ zone band and $|100\rangle$ belt band is too low efficient to dissipate heat (of hydrogen fusion), so it is broken into countless of (random distributed) micro convection spots. So the hydrogen fusion's heating blurs this $|211\rangle$ circulation effect. The fact that Sun's spin speed faster at equator (~ 25 days) than at pole (~ 34 days) supports this model. The Sunspot's butterfly pattern is also support this model, because in Babcock's magnetic-dynamo model^[7], the underneath layer has to spin faster than the surface layer. In this way, Sun's surface atmospheric circulation can also be explained by Schrodinger equation's solution and the QM peaking/depleting effect. A complete radial probability density (mass) distribution for Solar system from $\{-2,n\}$ super-shell to $\{2,n\}$ super-shell constructed by using Schrodinger equation solution is shown in Figure 4 of paper SunQM-3s1.

V. Other planets' atmospheric circulation pattern

Neptune (and Uranus) has $p\{N,n//2\}$ QM structure, a Earth-sized core at $p\{-1,1//2\}$. Its atmosphere starts at $p\{-1,1\}$ and ends at $p\{-1,2//2\}$, and has high mass occupancy, so it has a embedded $|211\rangle$ ring within $r/r_1 = 4$ (using r of $p\{-1,1\}$ as r_1). Therefore the "big picture" of Neptune (and Uranus) surface atmospheric circulation is dominated by the embedded $|211\rangle$

state, which should cause a major (very broad) zonal band at equator with faster eastward wind, and two small zonal bands at latitude $\theta' \approx \pm 60^\circ$.

Venus, Mars, and Mercury have $p\{N, n/2\}$ QM structure. Theirs atmosphere is out of the solid planet surface, so it sits outside of $r/r_1 = 4$ (with planet's core $p\{-1, 1/2\}$ as r_1), and it has $< 1\%$ (or relatively low) mass occupancy, so it quickly disappeared at above the planet's surface. Therefore the "big picture" of these planets' atmospheric circulation is dominated by the $|211\rangle$ state (not embedded, like Earth). which should cause a major uprising band at equator with faster eastward wind, and two small uprising bands at latitude $\theta' \approx \pm 60^\circ$.

Conclusion

Using $p\{N, n\}$ QM model with QM induced mass peaking/depleting effect, plus the spin frame of $\omega_{n\text{-spin}} \approx \omega_{1\text{-spin}} / n^3$, plus the multiplier n' , we successfully explained the origin of Jupiter surface cloud bands as the $|544\rangle$ state's QM peaking/depleting effect. We can even estimate how deep the convection starts below the atmosphere surface. The same analysis shows that the Earth's atmospheric circulation is caused by $|211\rangle$ state QM peaking effect at equator (major) and $\pm 60^\circ$ (minor), and QM mass depleting effect at $\approx \pm 35^\circ$ latitude. The result matches to the observed data very well. Furthermore, the same analysis resulted a "big picture" of atmospheric circulation for all planets (and Sun), and it matches to the real data reasonably well. All these results have provided more evidences that the $p\{N, n\}$ QM model with Schrodinger equation solution is a valid theory.

References

- [1] A series of my papers that to be published (together with current paper):
 SunQM-1: Quantum mechanics of the Solar system in a $\{N, n/6\}$ QM structure.
 SunQM-1s1: The dynamics of the quantum collapse (and quantum expansion) of Solar QM $\{N, n\}$ structure.
 SunQM-1s2: Comparing to other star-planet systems, our Solar system has a nearly perfect $\{N, n/6\}$ QM structure.
 SunQM-1s3: Applying $\{N, n\}$ QM structure analysis to planets using exterior and interior $\{N, n\}$ QM.
 SunQM-2: Expanding QM from micro-world to macro-world: general Planck constant, H-C unit, H-quasi-constant, and the meaning of QM.
 SunQM-3: Solving Schrodinger equation for Solar quantum mechanics $\{N, n\}$ structure.
 SunQM-3s1: Using 1st order spin-perturbation to solve Schrodinger equation for nLL effect and pre-Sun ball's disk-lyzation.
 SunQM-3s2: Using $\{N, n\}$ QM model to calculate out the snapshot pictures of a gradually disk-lyzing pre-Sun ball.
 SunQM-3s3: Using QM calculation to explain the atmosphere band pattern on Jupiter (and Earth, Saturn, Sun)'s surface.
 SunQM-3s6: Predict radial mass density distribution for Earth, planets, and Sun based on $\{N, n\}$ QM probability distribution.
 SunQM-5: C-QM (a new version of QM based on interior $\{N, n\}$, multiplier n' , $|R(n, l)|^2 |Y(l, m)|^2$ guided mass occupancy, and RF) and its application from string to universe.
 SunQM-5s1: White dwarf, neutron star, and black hole re-analyzed by using C-QM.
- [2] The citation of wiki "Solar core" means it is obtained from the Wikipedia online searching for "Solar core". Its website address is: https://en.wikipedia.org/wiki/Solar_core. This website address can be generalized for all other searching items.
- [3] From wiki "Atmosphere of Jupiter": by Sakurambo at English Wikipedia - Transferred from en.wikipedia to Commons by Shizhao using CommonsHelper. Own work based on :Image:Jupiterbands.JPG (uploaded by User:Erimus). Copy right: Public Domain.
- [4] From wiki "Atmosphere of Jupiter": Figure "Zonal wind speeds in the atmosphere of Jupiter", by Ruslik0 - Own work, Zonal wind speeds in the atmosphere of Jupiter. The results of the Voyager and Cassini missions are shown. The shaded

areas correspond to the locations of belts. Source: Vasavada, Ashvin R.; Showman, Adam (2005). "Jovian atmospheric dynamics: an update after Galileo and Cassini". *Reports on Progress in Physics* 68: 1935–1996. Copy right: CC BY-SA 3.0

[5] From wiki "Planetary core", Figure "The internal structure of the outer planets". Lunar and Planetary Institute - <https://solarsystem.nasa.gov/galleries/gas-giant-interiors>. Copy right: Public Domain.

[6] From wiki "Atmosphere of Earth", Figure "An idealised view of three large circulation cells". By DWindrim - Own work. Copy right: CC BY-SA 3.0

[7] From wiki "Babcock Model".

[8] Major QM books, data sources, software I used for this study are:

Douglas C. Giancoli, *Physics for Scientists & Engineers with Modern Physics*, 4th ed. 2009.

John S. Townsed, *A Modern Approach to Quantum Mechanics*, 2nd ed., 2012.

David J. Griffiths, *Introduction to Quantum Mechanics*, 2nd ed., 2015.

Stephen T. Thornton & Andrew Rex, *Modern Physics for scientists and engineers*, 3rd ed. 2006.

James Binney & David Skinner, *The Physics of Quantum Mechanics*, 1st ed. 2014.

Wikipedia at: <https://en.wikipedia.org/wiki/>

Online free software: WolframAlpha (<https://www.wolframalpha.com/>)

Online free software: MathStudio (<http://mathstud.io/>)

Free software: R

Microsoft Excel.

Public TV's space science related programs: PBS-NOVA, BBC-documentary, National Geographic-documentary, etc.

Journal: Scientific American.